All-Printed Green Micro-Supercapacitors Based on a Natural-derived Ionic Liquid for Flexible Transient Electronics

Lorenzo Migliorini,* Claudio Piazzoni, Kaija Pohako-Esko, Marta Di Girolamo, Andrea Vitaloni, Francesca Borghi, Tommaso Santaniello, Alvo Aabloo, and Paolo Milani*

The fabrication and characterization of green, flexible, and ultra-thin supercapacitors that are able to operate above 1.5 V is reported, using an all-printed fabrication process. The devices are produced by aqueous spray casting of a natural-derived electrolyte ionogel composed by 2-hydroxyethyl cellulose and by the ionic liquid choline lactate, while the electrodes are composed of highly porous nanostructured carbon films deposited by supersonic cluster beam deposition (SCBD). The obtained supercapacitors (device thickness < 10 μm) are stable to bending and they possess power values up to 120 kW kg^{-1}. The combination of aqueous spray casting and SCBD constitutes a versatile, scalable, and eco-friendly fabrication process able to directly print interconnected elements suitable for transient electronic systems.

1. Introduction

Organic and printed soft electronics play an increasingly important role enabling applications in many fields and in particular in the healthcare, environmental, and well-being industry.[1–3] This demands for the decreasing of the size and weight of the devices, the lowering of power demand, the improvement in cost competitiveness, lifetime and processability as well as up-scaling for a larger manufacturing capability.[4] Of crucial importance is the environmental impact of materials, fabrication processes, and lifecycle sustainability.[5,6]

Transient electronics (or biodegradable electronics) is an emergent technology that relies on the design and fabrication of devices able to dissolve or biodegrade in physiological and environmental media.[7,8] Based on renewable raw materials, transient electronics constitute a fundamental leverage of innovative solutions for bioresorbable medical implants with enhanced therapeutic and diagnostic performances.[6,9,10] In precision agriculture[11–13] and environmental monitoring,[14] extremely large numbers of biodegradable sensors and actuators can be deployed without worrying about their recovery. Considering also the globally increasing demand for portable electronic devices, biodegradability represents a necessary requisite for minimizing the environmental impact.[5,15,16]

In this context, eco-friendly batteries and supercapacitors (SCs) based on biodegradable components can play a key role as green energy storage devices (ESDs) to enable off-line operability.[17–19] Supercapacitors consist of a couple of high-surface area electrodes, usually made by porous carbon materials (graphene, nanotubes, active carbon)[20–27] and a liquid/solid electrolyte medium. Compared to other ESDs like batteries, SCs are characterized by higher power and lower complexity, making them ideal candidates for energy storage in wearable devices and miniature environmental sensors.[28] In order to achieve an effective sustainability for real applications, many challenging issues must be addressed concerning materials, performances, and production methods. In particular only natural and biodegradable raw materials should be used: recently cellulose and bioplastics such as poly(3-hydroxybutyrrate) have been proposed as solid polymeric matrices for supercapacitors,[29–34] however the issue of biodegradability and biocompatibility remains for the electrodes and the electrolytes. For example, the use of carbon nanotubes nanocomposites as electrodes is problematic, since the impact on the environment is still to be fully understood and potentially dangerous.[35] Ionic liquids have been widely employed as electrolytes for supercapacitors, thanks to their negligible volatility and good ionic conductivity,[36–39] however they are usually based on cytotoxic cations such as imidazolium heterocycles.[40–43]

Recent papers reported about biodegradable, flexible and miniaturized supercapacitors.[33,44–49] In these devices the electrolytes are composed by polysaccharide hydrogels (agarose, cellulose, flour) or polyvinyl alcohol, obtained by solution casting/coating technique. The electrodes are made by using metals and metal oxides (W, Fe, Mo, Mn, Ti, Zn),[33,45,47] active carbon[44,46] or poly(3,4-ethylenedioxythiophene) polystyrene

Dr. L. Migliorini, Dr. C. Piazzoni, M. Di Girolamo, A. Vitaloni,
Dr. F. Borghi, Dr. T. Santaniello, Prof. P. Milani
Interdisciplinary Centre for Nanostructured Materials
and Interfaces (CIMaINa)
Department of Physics
University of Milan
Via Celoria 16, Milan 20133, Italy
E-mail: lorenzo.migliorini@unimi.it; paolo.milani@mi.infn.it
Dr. K. Pohako-Esko, Prof. A. Aabloo
Institute of Technology
University of Tartu
Nooruse 1, Tartu 50411, Estonia

The ORCID identification number(s) for the author(s) of this article can be found under https://doi.org/10.1002/adfm.202102180.

sulfonate (PEDOT:PSS) and graphene oxide.[48] Organic conductive polymers such as PEDOT are biocompatible but not biodegradable.[50–52]

The use of water-based electrolytes appears as a suitable choice towards biodegradability, however it limits the working potential to values usually lower than 1 V, reducing as well the associated delivery power (it was reached a maximum specific power of 6 kW kg^{-1} of electrode material).[44] It would be highly desirable to obtain power values of at least 10 kW kg^{-1}, typical for commercial available supercapacitors.[53]

Fabrication processes compatible with non-conventional substrates (polymers and textiles) are also of primary importance for the device footprint: they should be eco-friendly, organic solvent-free, and suitable for micro-patterning of different geometries. Recently, printing techniques such as inkjet printing, screen printing and gravure printing have been employed for the fabrication of thin conductive films on different flexible substrates for different applications, like energy storage, photovoltaics and optoelectronics.[54–56] This additive manufacturing approach can solve the problem of scalability and can ensure an efficient large-area patterning with low raw material consumption. Conductive inks have been designed and developed for this purpose, usually based on viscous stable suspensions of conductive nanostructures, such as metallic nanoparticles or nanowires, graphene and conductive polymers.[57] Nevertheless, the conceptual simplicity of this approach encounters with some issues. The employed inks must simultaneously achieve high loading of the conductive species, suspension stability and suitable viscosity, so that the presence of stabilizers, thickeners and additives is often required.[58] The inks can show a poor affinity with the substrate of choice, making mandatory surface activation pre-treatments like plasma oxygen. Moreover, the printed patterns often require heat post-treatments to achieve suitable electronic conductivity, which is particularly inappropriate for thermolabile substrates such as many natural-derived biodegradable materials.

As an alternative to traditional printing technologies, supersonic cluster beam deposition (SCBD) has been proposed as an additive manufacturing technique based on the gas-phase generation of cluster beams and in their controlled deposition on various rigid and flexible surfaces.[59–62] The use of solid precursors, sputtered in vacuum, avoids the use of any solvent, moreover the high collimation of the supersonic cluster beam is suitable for stencil mask-assisted micropatterning, allowing a fine control on the thickness and the roughness of the deposited nanostructured films[63] together with a robust adhesion and resiliency to mechanical deformation.[64,65] SCBD is a room-temperature technique that allows the use of thermolabile and/or easily degradable materials and substrates with no pre- or post-treatments.[66–72]

Here we report about a fully natural-derived, flexible, and ultra-thin micro-supercapacitor able to operate above 1.5 V and obtained with an all-printed fabrication process. We used a ionogel electrolyte composed by 2-hydroxyethyl cellulose (HEC) and the biodegradable ionic liquid choline lactate (CL),[43,73] whose window of electrochemical stability is of 1.6 V. The electrodes are constituted by highly porous nanostructured carbon films. The layer-by-layer fabrication process is based on printing technologies suitable for scalability and micro-patterning.[74]

More specifically, devices with thickness < 10 μm are obtained through the combination of water-based spray casting and solvent-free supersonic cluster beam deposition technique. We performed a full electrochemical characterization of the devices, both in ambient and inert atmosphere, varying the ionic liquid's amount and the carbon electrode thickness. The supercapacitors also underwent bending, cyclic, and dissolution tests. The direct production of devices in series and parallel connection is also shown.

2. Results and Discussion
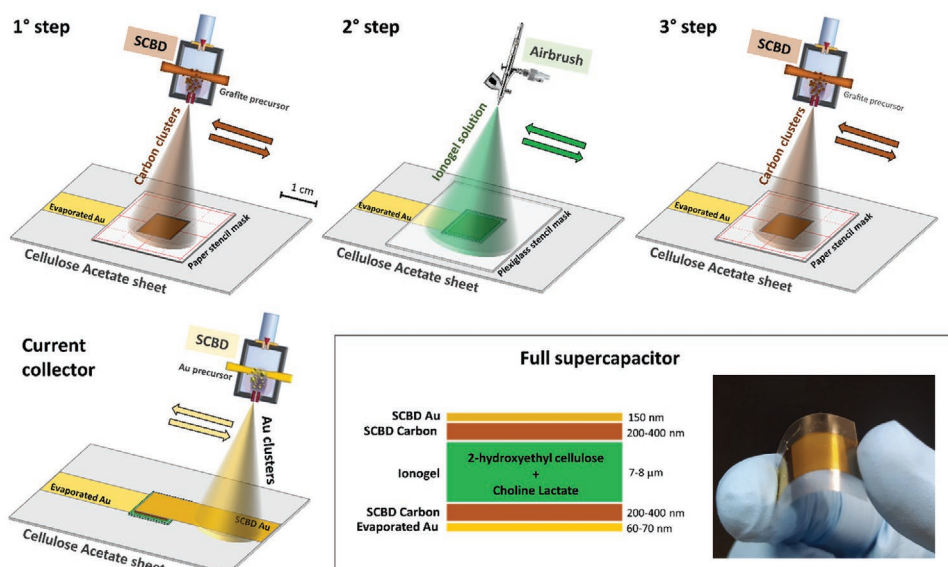
2.1. Layer-By-Layer Printing Process

Eco-friendly and biodegradable reagents and materials were employed for the formulation and the fabrication of the supercapacitors. The natural-derived ionogels were obtained by blending 2-hydroxyethyl cellulose (HEC) with the ionic liquid choline lactate (CL). The last was synthesized through a simple acid-base reaction between choline bicarbonate and lactic acid carried out in water solution. Both were dissolved in distilled water. The active electrodes were composed solely by highly porous cluster-assembled carbon films, obtained from a graphite precursor with a solvent-free physical vapor deposition process. The steps of the fabrication are reported in **Figure 1**.

It consists in a layer-by-layer printing process that combines spray casting and supersonic cluster beam deposition. The substrates were transparent and flexible biodegradable sheets of cellulose acetate (CA), preventively provided with a conductive evaporated Au film (60–70 nm) to serve as bottom current collectors. The first fabrication step involved the deposition of the bottom carbon electrode (0.8 × 0.8 cm²) by means of SCBD. Both 200 and 400 nm-thick electrodes were deposited to study how this could affect the electrochemical and energetic performances of the device (C200 and C400 samples). Their mass was of 10 and 20 μg cm^{-2}, respectively.

The second step was the spray casting of the biodegradable ionogel (1 × 1 cm²) using a standard airbrush mounted in place of the extruder of a 3D printer, so that the process could be controlled with a dedicated g-code. The spray beam was rastered above the target 600 times to reach a final thickness of 7–8 μm. Two different types of ionogel were casted, varying the mass percentage of the choline lactate: CL60% and CL70%. The third step was the deposition of the top carbon electrode by SCBD. Finally, a thin Au film (150 nm) was also deposited via SCBD as the top current collector. The full supercapacitors were very thin (<10 μm) and lightweight (≈0.9 mg cm^{-2}): these are crucial features for flexible electronics applications. The entire fabrication process was conducted at room temperature and employing only water as solvent.

### 2.2. Morphology, Imaging, and Dissolution Tests

Stylus profilometry was employed to measure the thickness of different CL70% ionogels after 200, 400 and 600 rastering steps of the spray casting process. **Figure 2a** shows the corresponding average thickness values of ≈1.5, 4.5, and 7.5 μm,

Figure 1. Schematization of the supercapacitors layer-by-layer printing process. The substrate is a cellulose acetate flexible sheet. Carbon electrodes were obtained by SCBD, while the ionogel by spray casting. Au thin films were also deposited by mean of physical vapor deposition (PVD) and SCBD technique. An insight on the layer's thickness values and a photo of the resulting flexible device are also reported.

demonstrating how the spray casting process can be easily controlled at the microscale. Figure 2b shows a pseudo-3D map of the 7.5 µm-thick CL70% ionogel that allowed to calculate a roughness value of 0.67 µm. The morphology of the carbon cluster-assembled electrodes was examined by atomic force microscopy (AFM). The first picture of Figure 2c shows the surface of the bottom 400 nm-thick electrodes, that have been deposited on the flexible substrate. The calculated roughness
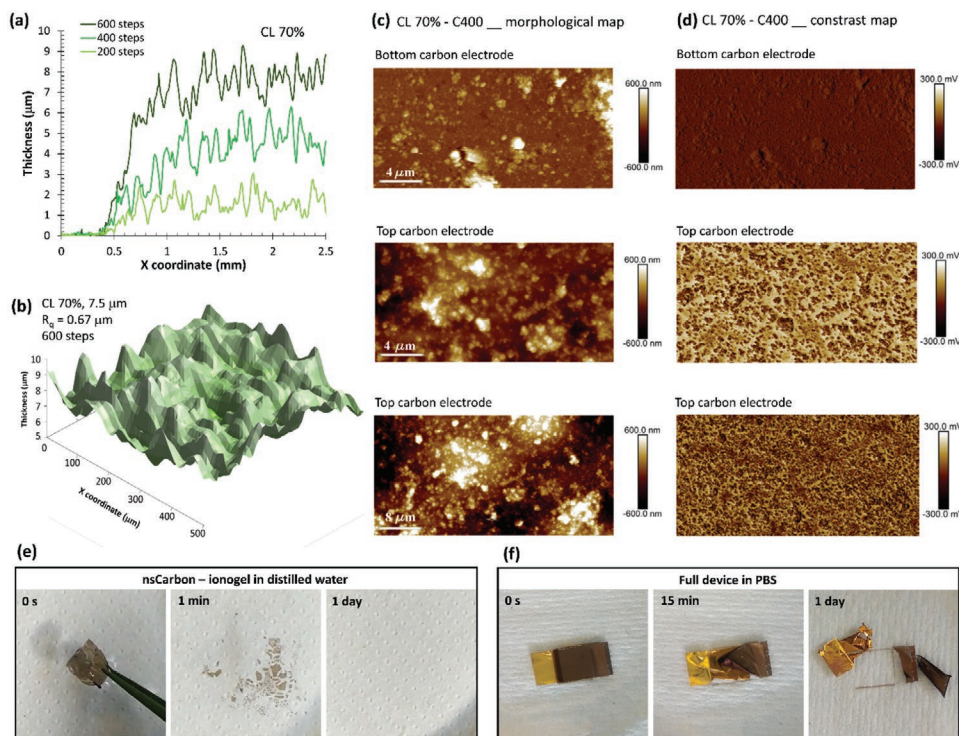
Figure 2. a) 2D profile of the CL 70% ionogel at 200, 400, and 600 rastering steps of the spray casting process; b) Pseudo-3D map of the CL 70% ionogel's surface after 600 rastering steps; c) AFM morphology; and d) the corresponding phase maps of cluster-assembled 400 nm-thick carbon films. The first row shows the surface of the bottom carbon electrode (deposited on the rigid substrate), while the second and the third show the top carbon electrode deposited on the surface of the ionogel, with different magnifications; e) Dissolution of a free-standing supercapacitor in distilled water; f) Dissolution of the full device in PBS.

**ADVANCED
SCIENCE NEWS**

www.advancedsciencenews.com

**ADVANCED
FUNCTIONAL
MATERIALS**

www.afm-journal.de

was 133 ± 11 nm, while it was 103 ± 8 nm for the 200 nm-thick (3D and 2D maps are also reported in Figure S1, Supporting Information). These high values arise since clusters organize at the nano and mesoscale on the substrate, by providing morphological properties to the thin film which evolve with the quantity of mass deposited (which is proportional to the film thickness), according to a simple scaling law.[62] The specific surface area ($A_{BET} \approx 1500$ m^2 g^{-1}) is almost constant with the film thickness,[62] while the effective surface area increases with the quantity of mass deposited, ideally leading to higher C_{dl} values.[75]

The corresponding picture in Figure 2d is a phase map that stress the contrast in the chemical composition: as can be seen, the carbon clusters homogeneously cover the underlying substrate. The second and the third pictures of Figure 2c,d refers instead to the surface of the top carbon electrodes, deposited on top of the biodegradable ionogel thin films. In this case, considering the phase maps, it appears that the carbon clusters did not simply deposited on the gel surface. Instead, a composite phase is formed where the clusters are partially embedded into the gel medium, which can be due to their implantation underneath the gel surface during the deposition process, or alternatively to the diffusion of the ionic liquid inside the pores of the already formed carbon film. The formation of a composite phase characterized by a tight interaction between the electrolyte gel and the electrodes should lead to the formation of a high interfacial area, which is a strategic feature to obtain high values of double layer capacitance C_{dl}.

Since the presented supercapacitors have been designed for applications in transient electronics, we tested their behavior when immersed in physiological and/or environmental media.[7,8] For this purpose, two different dissolution tests were carried out, similar to those reported in other works.[19,45,47,49] Initially, the dissolution of a free-standing CL70%-C400 supercapacitor was tested in distilled water (Figure 2e), showing fast fragmentation in <1 min. The day after, no visible traces were observed in the Petri dish, meaning that all the fragments completely dissolved. This result was consistent with the structure of the cellulose-choline lactate ionogel, where no chemical bonds are formed during the synthesis thus allowing water molecules to pervade the polymeric matrix, unfolding the chains, and leading to dissolution. A second test was carried out by immersing a full device (cellulose acetate substrate – supercapacitor – current collectors) inside a physiological phosphate buffer solution (PBS) (Figure 2f). After 24 h, the gold current collectors fully disassembled from the substrate, leaving the ionogel free to be permeated by the solution and to completely dissolve. The obtained results in both water and PBS proved the suitability of these novel supercapacitor to be integrated in transient electronic devices able to benignly dissolve without leaving traces in aqueous and physiological media. Moreover, if necessary, the biodegradation of cellulose and choline lactate by microorganisms have already been extensively studied and assessed.[43,73]

## 2.3. Electrochemical and Energetic Characterization

In a dry environment, the interactions between the ionic liquid and the electrode's surface determine the electrochemical

parameters of the supercapacitors, such as the double-layer capacitance (C_{dl}), the equivalent series resistance (ESR) and the maximum working potential.[76] Considering that choline lactate is a highly hydrophilic ionic liquid, the presented ionogels spontaneously absorbs water molecules from humid atmosphere, leading to a partial ionic solvation that can affect all the aforementioned electrochemical parameters. Therefore, the supercapacitors were electrochemically tested in ambient humid conditions as well as in inert and dry nitrogen atmosphere, to study their behavior in both the situations.

CL60%-C200 and CL70%-C200 initially underwent electrochemical impedance spectroscopy (EIS) in ambient conditions and they provided the same result: nice capacitive behavior and an equivalent series resistance (ESR) of ≈9 Ω cm^2 (the blue line in **Figure 3a**). Cyclic voltammetry (CV) was carried out as well and 0.9 V showed to be the maximum working potential in a humid environment, since at higher ΔV electrochemical reactions took place. Also in this case, no difference could be spotted amongst the two different formulations (the blue line in Figure 3b). Considering the hygroscopicity of both the employed cellulose and ionic liquid, we can easily assume that the absorbed humidity in ambient conditions solvates the choline lactate ions, leading to an equal ionic migration and double-layer capacitance.

The same samples were also tested in inert nitrogen atmosphere and they showed a completely different behavior (green lines in Figure 3a,b). Without ambient humidity the ions of the ionic liquid were not solvated, they lose mobility and the influence of IL mass percentage was evident: the ESR values increased up to 150 Ω cm^2 for CL70%-C200 and up to 310 Ω cm^2 for CL60%-C200. More significantly, the electrochemical stability window reached 1.6 V, a crucial benefit to increase the stored energy and the delivery power of the devices. A working potential above 1 V is quite usual regarding supercapacitors with heterocycles-based ionic liquid (like imidazolium-based ones), whereas biodegradable supercapacitors that usually employ aqueous electrolytes are characterized by a potential lower than 1 V.

Since the CL70% ionogels showed to be more performant than the CL60% ones, we deposited 400 nm-thick carbon electrodes (CL70%-C400) in order to check how the electrodes thickness and roughness could affect the electrochemical and energetic properties (Figure 3a,b). The obtained ESR value of 160 Ω cm^2 was slightly higher than those of its 200 nm counterpart. This can be due to the intrinsic internal resistance of the carbon electrodes: the higher thickness also resulted in a higher ESR. It can also be caused by the higher roughness (measured by AFM), since certain portions of the electrode surface are likely to be more difficult to reach for the IL ions and this can lead as well to an increase in the ESR. From the CV it can be seen how the CL70%-C400 provided the highest capacitive current and this too is coherent with the higher thickness, roughness, and surface area of the carbon electrodes. A common feature of all the formulations was the good capacitive behavior when subjected to CVs over a wide range of scan rate (from 50 to 3 V s^{-1}). The CV curves related to CL70%-C400 are shown in Figure 3d, others can be found in the Supporting Information (Figures S2–S5, Supporting Information).
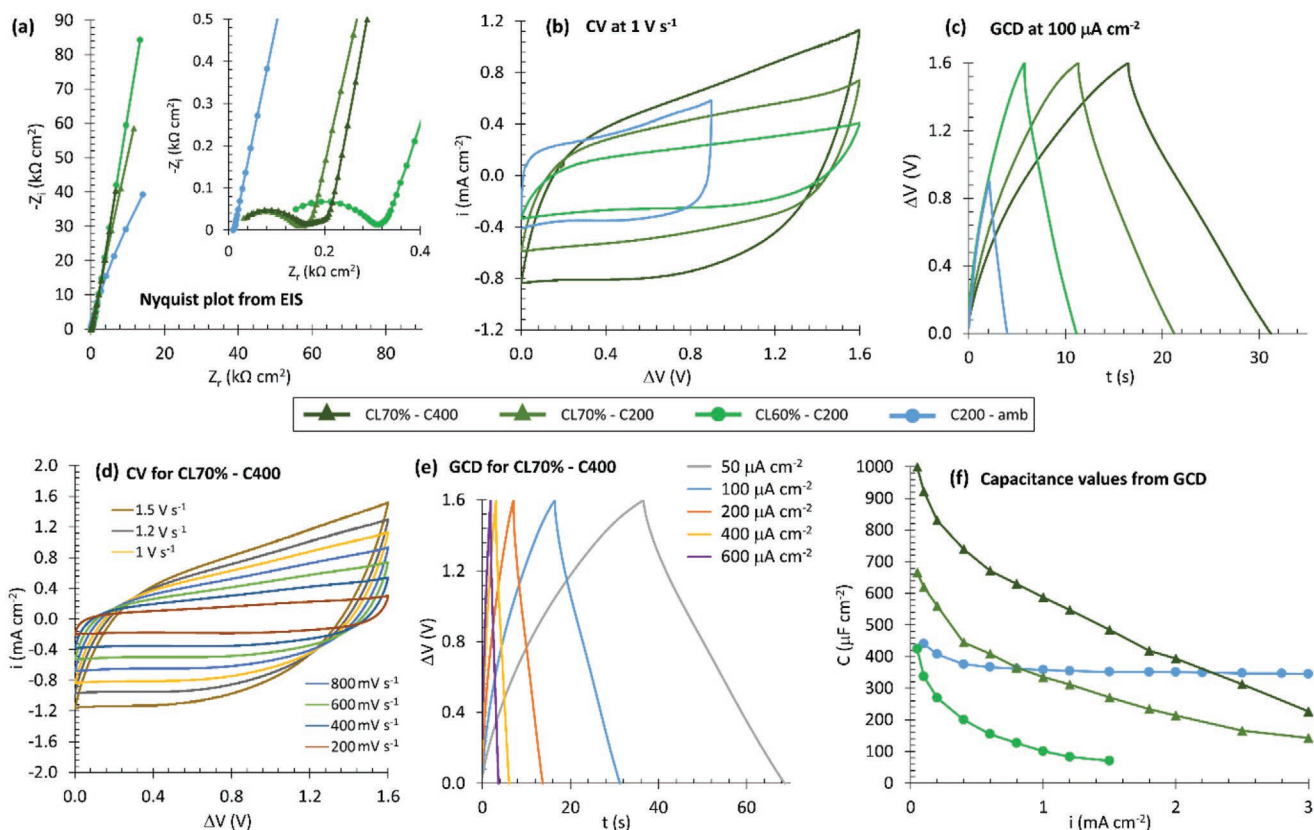
Figure 3. a) EIS, b) CV, and c) GCD carried out on the different samples. The plots of CL60%-C200 and CL70%-C200 tested in ambient conditions showed to be completely superimposable and they are then represented as a single blue line; the three different green lines represent the samples CL60%-C200, CL70%-C200, and CL70%-C400 tested in inert atmosphere. c) CV curves at different scan rates obtained from the CL70%-C400 sample in inert atmosphere; e) GCD curves at different current values obtained from the CL70%-C400 sample in inert atmosphere; f) A graph showing for each sample how the double-layer capacitance varies accordingly to the GCD applied current value.

Galvanostatic charge and discharge (GCD) cycles were also carried out on all the samples confirming the already observed behavior (Figure 3c). The samples have been charged up to a ΔV of 0.9 V in ambient conditions and of 1.6 V in inert atmosphere. The time of charge (t_c) and of discharge (t_c) increased for higher mass percentage of ionic liquid and for thicker carbon electrodes. The applied current density ranged from 50 µA cm^{-2} to 3 mA cm^{-2} and Figure 3e reports the GCD curves related to the sample CL70%-C400. Other low-current GCD are reported in Figure S6–S8, Supporting Information. The double-layer capacitance (C_{dl}) values were extracted from the GCD curves for every sample at every tested current (Figure 3f). In all cases, C_{dl} increased for lower applied currents and it decreased for higher ones, as typical for supercapacitors. The samples tested in ambient conditions showed a better rate performance and higher capacitance at high currents (350 µF cm^{-2} at 3 mA cm^{-2}): this is due to their lower ESR (as extracted from the Nyquist plot) resulting as well in a lower voltage drop during the discharge curve at high rate/currents. The tests in inert atmosphere resulted in very high values of C_{dl} especially for low applied currents and, as expected from previous tests, they increased with the IL mass percentage and the electrodes thickness, reaching high maximum values of 424 µF cm^{-2} for CL60%-C200, 666 µF cm^{-2} for CL70%-C200 and 1 mF cm^{-2}

for CL70%-C400. Columbic efficiency (CE) was always >90% at low currents and >95% at higher ones. C_{dl} values were also calculated from CV curves (see Figure S9, Supporting Information) and they showed to be coherent. GCD curves were employed to calculate the specific stored energy E_s and average delivery power P_s (E and P normalized per the electrodes mass) as well as their areal counterparts E_A and P_A (normalized per the electrodes occupied area).

Figure 4a shows a Ragone plot where the obtained specific energy and power are reported and compared with other biodegradable and flexible micro-supercapacitors reported in the literature. E_s and P_s increased shifting from the 60% to the 70% IL mass percentage, but this was not the case when the electrodes thickness was increased from 200 to 400 nm. In fact, the electrodes mass doubled while the capacitance gain was of about the 60% of its original value. Because of this, CL70%-C200 was the best candidate in terms of specific energy and power, reaching maximum values of 11.8 Wh kg^{-1} and 120 kW kg^{-1}. As can be seen from the comparison with other works,[33,44–49] the present supercapacitors are characterized by the highest specific delivery power and by a very good specific stored energy. These results are mainly due to the high surface area of the nanostructured carbon electrodes and by the electrochemical stability of the choline lactate up to 1.6 V, which is a
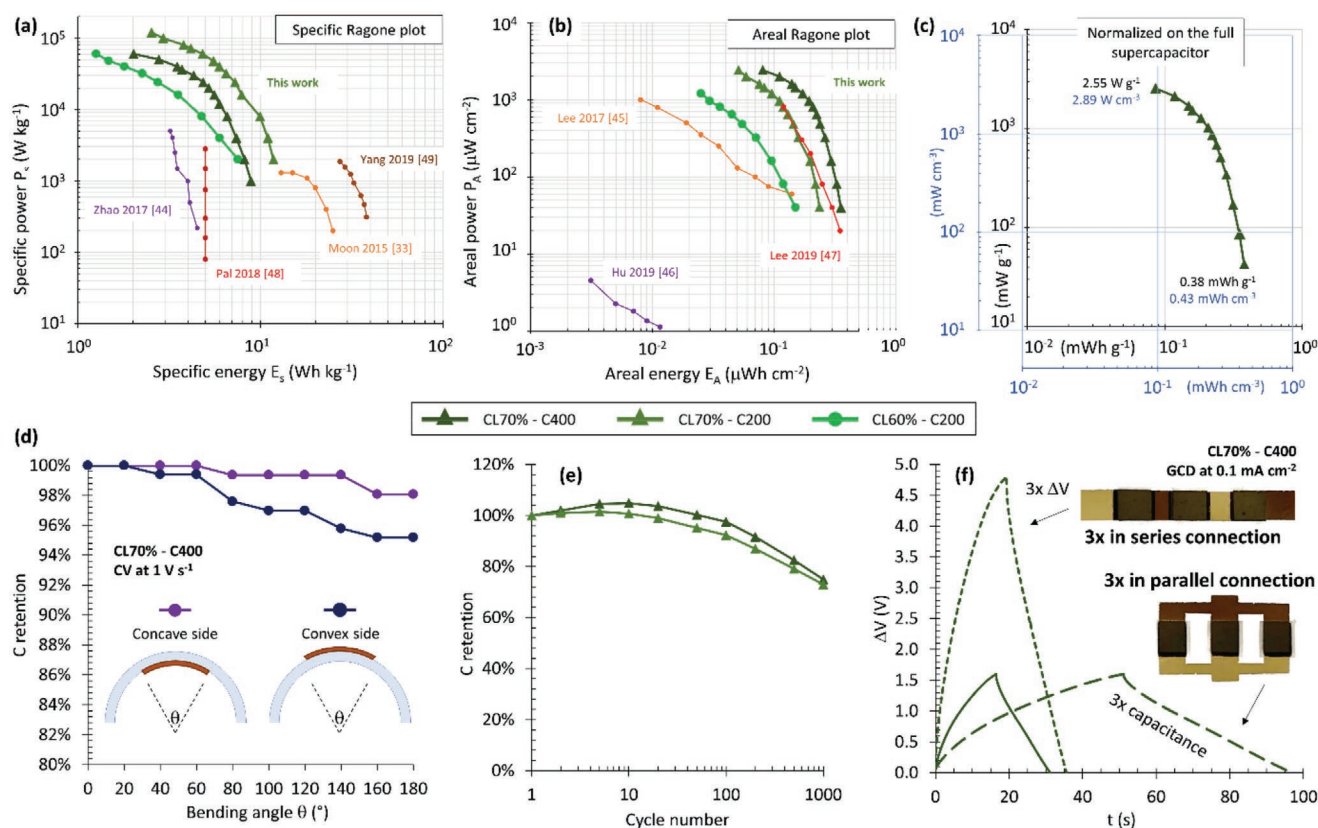
Figure 4. a–b) Ragone plot reporting the supercapacitors stored energy and average delivery power normalized by the electrodes mass and occupied area (respectively) and compared to other state of the art works; c) Obtained energy and power normalized by the mass and the volume of the full supercapacitor; d) Graph reporting the capacitance retention as a function of the bending degree at which the supercapacitor was subjected (both on the concave and convex side); e) Graph reporting the capacitance retention of the supercapacitors under the effect of 1000 CV cycles at a scan rate of 800 mV s^{-1}; f) GCD curves obtained from a single CL70%-C400 supercapacitors and from three of them connected both in series and in parallel; top photographs of the samples are also shown: the darker areas are the ionogels sandwiched between the carbon electrodes, the brownish areas are SCBD Au films while the yellow ones are the Au current collectors obtained by thermal evaporation.

significative energetic boost with respect to other biodegradable supercapacitors based on aqueous electrolytes.

Energetic parameters normalized per electrode area (E_A and P_A) are shown in Figure 4b. In this case, thicker electrodes led to an increase in the double-layer capacitance without changing the area on the substrate and then the best candidate is represented by CL70%-C400, reaching maximum values of 0.36 µWh cm^{-2} and 2.4 mW cm^{-2}. Such values are on the edge of state-of-the-art green supercapacitors and areal performances are particularly relevant for applications in planar microdevices where the occupied surface is of crucial importance. Because of this, the obtained energy and power were also normalized by the mass and the volume of the complete supercapacitor, that is by considering not only the electrodes but also the electrolyte medium. The results are shown in Figure 4c. The maximum obtained energy values were of 0.38 mWh g^{-1} and 0.43 mWh cm^{-3}, while the maximum obtained average delivery powers were of 2.55 W g^{-1} and 2.89 W cm^{-3}. In all the cases, the energetic performances of the supercapacitors tested in ambient atmosphere showed to be lower because of the drop in the working potential (from 1.6 to 0.9 V). Their Ragone plot is shown in Figure S10, Supporting Information.

Electromechanical flexibility tests were carried out by performing CV analyses while bending the substrate together with the printed supercapacitor. As can be seen from the graph in Figure 4d, the obtained supercapacitors showed an excellent stability to bending up to 180 degrees with the supercapacitor on both the concave and convex side, with a capacitance retention C_r always >96%. Cyclic stability was also tested by monitoring the capacitance retention up to 1000 cycles of the samples CL70%-C200 and CL70%-C400. The capacitance slightly increased during the first ten cycles but then it decreased, reaching a C_r value of ≈75% at 1000 cycles (the corresponding graph is reported in Figure 4e). We assume that during the first ten cycles, a reorganization of the carbon clusters allows to host a higher amount of charge. The subsequent decrease in the double-layer capacitance is likely to be the consequence of the gradual saturation of some of the electrode pores.

In order to test the capability of the proposed approach to print structures with different geometries and connections, three different supercapacitors were printed in a single process and tested both in series and in parallel. GCD tests were carried out on the connected supercapacitors and the results are shown in Figure 4f, together with photographs of the connected devices. The series connection of three SCs led to a device able

to operate up to 4.8 V, while the parallel connection allowed to obtain a triple double-layer capacitance ($\approx$3 mF cm^{-2}). A schematization of the device connection design is provided in Figures S11, S12, Supporting Information. No post-processing or wiring of the different elements was needed after the fabrication.[33,44,49]

3. Conclusions

This work demonstrates the fabrication and characterization of natural-derived flexible and ultra-thin micro-supercapacitors able to operate at 1.6 V and obtained with a few-step all-printed automated fabrication process. 2-hydroxyethyl cellulose and choline lactate constitute the ionogel electrolyte, obtained with a water-based spray casting technique. The thin electrodes are composed by highly porous nanostructured carbon, deposited with solvent-free SCBD technique. The effect of the ionic liquid amount and of the carbon electrode thickness was studied through electrochemical analyses in both ambient and inert atmospheres. The tested energetic performances reach delivery powers of 120 kW kg^{-1} (2.4 mW cm^{-2}) and stored energies of 11.8 Wh kg^{-1} (0.36 μWh cm^{-2}). Excellent stability to bending was also assessed. The layer-by-layer fabrication process, based on printing technologies, is completely eco-friendly and highly suitable for scalability, automation and micro-patterning. Complex structures consisting of supercapacitors in series and in parallel can be directly obtained with no need of subsequent electrical wiring. Thanks to their performances, natural derivation and lightness, as well as fast dissolution in aqueous solutions, our devices can constitute a valuable solution for energy storage functionalities in transient electronic systems finding applications in many strategic areas such as biomedicine, precision agriculture and environmental monitoring.

4. Experimental Section

Choline Lactate Synthesis: Choline lactate was synthesized from choline bicarbonate (Sigma-Aldrich, 80% in H$_2$O, used as received) and DL-lactic acid (Sigma-Aldrich, 85%, used as received) using an established method.[77] Lactic acid dissolved in water and choline bicarbonate solution were mixed in 1:1 molar ratio under ambient conditions for 12 h. Choline lactate was separated and purified by extraction with ethyl acetate and then dried in vacuo. The product was obtained as colorless viscous liquid with a quantitative yield. Water content of choline lactate determined by coulometric Karl Fischer titration (Mettler Toledo DL32) was <1 wt%. Structure of choline lactate was confirmed with ^{1}H NMR spectra recorded with a Bruker Advance II 400 MHz spectrometer using D$_2$O as a solvent.

^{1}H NMR (400 MHz, D$_2$O): δ 4.39-4.00 (q, 1H, HOCHCH$_3$CO$_2^-$), 4.00-3.98 (m, 2H, HOCH$_2$CH$_2$N$^+$(CH$_3$)$_3$), 3.46-3.43 (t, 2H, HOCH$_2$CH$_2$N$^+$(CH$_3$)$_3$), 3.13 (s, 9H, HOCH$_2$CH$_2$N$^+$(CH$_3$)$_3$), 1.38-1.24 (d, 3H, HOCHCH$_3$CO$_2^-$).

Preparation of the Substrate: The substrate of choices was 75 μm-thick transparent and flexible cellulose acetate (CA) sheets, purchased from Graphix Plastics. Their biodegradability is assessed by the manufacturer. They were provided with a 50 nm-thick Au film (16 $\times$ 8 mm) as current collector by means of thermal evaporation using an Edwards Coating System (model E306A).

Deposition of Carbon Electrodes: The 200 and 400 nm-thick bottom carbon electrodes were deposited on top of the thermally evaporated

Au films on the CA sheets (covering a surface of 8 $\times$ 8 mm). The top ones were similarly deposited on the surface of the electrolyte ionogel following the same experimental procedure. SCBD is an additive technology based on the production of intense and highly collimated nanoparticle beams that enables the large-scale and high throughput integration of nanostructured functional materials on a wide variety of substrates, including microfabricated platforms, smart nanocomposites and fragile materials.[59,64,78–81] The assembling of carbon nanoparticles via SCBD is a suitable approach for the production of porous carbon thin films with structural and morphological properties that are beneficial for electrochemical applications.[82,83] The use of SCBD for the integration of carbon electrodes into conventional flexible substrates (e.g., Mylar) for the fabrication miniaturized devices, such as supercapacitors and electrolyte gated transistors, had been reported.[67,84]

SCBD consists in the room temperature deposition of nanoparticles accelerated in a free jet expansion of an inert carrier gas under high vacuum conditions, thus forming a cluster seeded supersonic beam. Carbon clusters are produced in a pulsed micro-plasma cluster source (PMCS) by the ablation of a graphite target. Details about operation principles of SCBD and PMCS can be found in ref. [59,85] When intercepting the cluster beam with a substrate, the nanoparticles stack and pile up randomly on the surface without fragmentation and form highly porous films.[62] Nanostructured carbon films deposited by SCBD consists in a high surface area disordered carbon with a very low-density ($\approx$0.5 g cm^{-3}) and high specific surface area ($\approx$1500 m^2 g^{-1}).[62,66,67] The high directionality of the cluster beam makes this technique particularly suitable to the design of patterned surfaces (with a lateral resolution down the micrometric scale) via the simple interposition of stencil masks.[79]

Ionogel Spray Casting: 2-hydroxyethylcellulose (90.000 Mw) (HEC) was purchased from Sigma Aldrich, while choline lactate (CL) was synthesized as previously described. HEC and CL were dissolved in distilled water inside a flask, keeping a constant cellulose concentration of 10 g L^{-1} and varying the amount of CL to have a HEC:CL mass ratio of 4:6 (CL60%) or 3:7 (CL70%). The solution was stirred for few hours and it was then injected in the reservoir of a conventional Gocheer airbrush. The volume of the reservoir was about 8 mL. A nozzle with a diameter of 0.5 mm was employed and the spray was operated with nitrogen at a pressure of 2 bar. A PowerWASP EVO (FFF – multifunction) 3D printer (category: FFF Cartesian, Single Bowden Extruder, Non-heated bed, Open chamber) was employed with the airbrush in place of the extruder, while the substrates were placed on the bottom moving plate. In this way, it was possible to use a g-code to control the rastering of the spray beam in a reproducible way, by keeping 18 cm between the nozzle and the substrates and a rastering speed of 8 mm s^{-1}. Plexiglass stencil masks with a 1 $\times$ 1 cm^2 hole were used to obtain a square shape of the sprayed ionogels. Some pictures of the employed instrumentation are reported in Figure S13, Supporting Information. The spray casting of the three SCs connected in series and the three SCs connected in parallel was carried out in a unique step and a representative design of their structure and interconnection is reported in Figure S11, S12, Supporting Information as well.

Deposition of the Top Current Collector: A 150 nm-thick Au current collector (16 $\times$ 8 mm) was deposited on top of the supercapacitor by means of supersonic cluster beam deposition, in a process quite analogous to the one employed for the deposition of the carbon electrodes. In this case, a gold rod was employed as the precursor for the Au nanoparticle generation.[60]

Morphology and Imaging: The morphological investigation of the carbon nanostructures was performed by a Multimode 8 AFM (Bruker), in Peak-Force Tapping Mode, equipped with silicon nitride cantilevers mounting single crystal silicon tips, with nominal radius 12–30 nm, resonance frequency in the range 100–200 kHz, and force constant k = 0.7 N m^{-1}. From flattened AFM images, the root-mean-square surface roughness R_q was calculated as the standard deviation of surface heights. The film thickness was calculated by scanning a region of the film deposited on a smooth silicon surface, where a sharp step was produced by masking the substrate during cluster deposition. The phase maps acquired by AFM provide the possibility to qualitatively stress a

contrast which can be attributed to the energy dissipation by materials of different composition on the surface, as also to different interfacial properties that affect the tip-sample interaction. A representative 3D AFM map of the topography and a height profile of the carbon thin film step was reported in Figure S1, Supporting Information, for each sample. All the topographic maps have been collected with a sampling resolution of 1–5 nm pixel^{-1} using a scan rate of ≈1 Hz. The surface of the ionogels was investigated by means of a stylus profilometer (KLA Tencor). 3D scans were performed on areas of 0.5×0.5 mm^2, with a load of 0.1 mg and a scanning speed of 0.2 µm s^{-1}.

Dissolution Tests: A free-standing CL70%-C400 sample, composed by the ionogel and the two carbon electrodes, was immersed in distilled water inside a Petri Dish and its dissolution was monitored by capturing photo with a conventional camera. A similar test was conducted with the immersion of a full supercapacitor device (also comprising the cellulose acetate substrate and the two gold current collectors) inside a Petri dish filled with phosphate buffer solution (PBS), prepared by dissolving in water the following salts: NaCl (8 g L^{-1}), KCl (2.7 g L^{-1}), Na$_2$HPO$_4$ (1.42 g L^{-1}), and KH$_2$PO$_4$ (0.24 g L^{-1}).

Electrochemistry: The analyses were performed with a Gamry potentiostat (model Reference 600) and a Gamry software. The tests in ambient conditions were carried out at 23 °C and RH = 50%. Inert atmosphere analyses were conducted inside a glove box filled with nitrogen (0.03 ppm of O$_2$). EIS analyses were carried out with an AC = 5 mV superimposed at a DC = 0 V, with a scanning frequency between 1×10^{-2} and 1×10^6 Hz. The ESR value was extracted from the Nyquist plot, more precisely from the intersection with the *X*-axis. CV and GCD analyses were carried out up to ΔV of 0.9 V (ambient conditions) or 1.6 V (inert atmosphere). CV scan rates ranged from 50 mV s^{-1} to 3 V s^{-1}, while GCD current densities from 50 µA cm^{-2} to 3 mA cm^{-2}. The areal C_{dl} (F cm^{-2}) was extracted from GCD curves according to Equation 1:

$$C_{dl} = \frac{i \times t_d}{\Delta V} \qquad (1)$$

where i is the current density, t_d the time of discharge and ΔV the working potential. The areal stored energy E_A (Wh cm^{-2}) and average delivery power P_A (W cm^{-2}) were calculated according to Equations 2 and 3, respectively:

$$E_A = \frac{C_{dl} \times \Delta V^2}{7200} \qquad (2)$$

$$P_A = \frac{3600 \times E}{t_d} \qquad (3)$$

The specific energy and power E_s and P_s were obtained by dividing E_A and P_A by the carbon electrodes mass. The energy and the power values reported in Figure 4c were obtained by normalizing per the mass and the volume of the full supercapacitors, composed by the two electrodes and the sandwiched electrolyte ionogel. The electromechanical bending tests were carried out with a custom assembled linear translator consisting of a step motor (28BYJ-48, 5V, DC), a rod bar and a moving support, controlled by an Arduino board. One end of the CA sheets, on which the supercapacitors were printed, was clamped to a fixed part of the translator, while the other end was moved towards through a linear displacement. In this way, the SCs were subjected to different bending angles both on the concave and convex side and for each of them a CV scan was carried out (scan rate of 800 mV s^{-1}). The capacitance retention C_r was calculated as the ratio between the C_{dl} value at a certain imposed angle and its original value without bending. Similarly, cyclic capacitance retention was calculated as the ratio between the C_{dl} value at a certain CV cycle and its original value during the 1st CV curve.

Supporting Information

Supporting Information is available from the Wiley Online Library or from the author.

Conflict of Interest

The authors declare no conflict of interest.

Data Availability Statement

The data that support the findings of this study are available from the corresponding author upon reasonable request.

[1] H. R. Lim, H. S. Kim, R. Qazi, Y. T. Kwon, J. W. Jeong, W. H. Yeo, *Adv. Mater.* **2020**, *32*, 1901924.

[2] L. Xiang, F. Xia, H. Zhang, Y. Liu, F. Liu, X. Liang, Y. Hu, *Adv. Funct. Mater.* **2019**, *29*, 1970339.

[3] Y. Liu, M. Pharr, G. A. Salvatore, *ACS Nano* **2017**, *11*, 9614.

[4] F. B. Kadumudi, M. Jahanshahi, M. Mehrali, T. G. Zsurzsan, N. Taebnia, M. Hasany, S. Mohanty, A. Knott, B. Godau, M. Akbari, A. Dolatshahi-Pirouz, *Adv. Sci.* **2019**, *6*, 1801241.

[5] J. Li, X. Zeng, A. Stevels, *Crit. Rev. Environ. Sci. Technol.* **2015**, *45*, 840.

[6] S. K. Kang, R. K. J. Murphy, S. W. Hwang, S. M. Lee, D. V. Harburg, N. A. Krueger, J. Shin, P. Gamble, H. Cheng, S. Yu, Z. Liu, J. G. McCall, M. Stephen, H. Ying, J. Kim, G. Park, R. C. Webb, C. H. Lee, S. Chung, D. S. Wie, A. D. Gujar, B. Vemulapalli, A. H. Kim, K. M. Lee, J. Cheng, Y. Huang, S. H. Lee, P. V. Braun, W. Z. Ray, J. A. Rogers, *Nature* **2016**, *530*, 71.

[7] R. Li, L. Wang, D. Kong, L. Yin, *Bioact. Mater.* **2018**, *3*, 322.

[8] J. Rossiter, J. Winfield, I. Ieropoulos, *Electroact. Polym. Actuators Devices 2016* **2016**, *9798*, 97981S.

[9] S. W. Hwang, X. Huang, J. H. Seo, J. K. Song, S. Kim, S. Hage-Ali, H. J. Chung, H. Tao, F. G. Omenetto, Z. Ma, J. A. Rogers, *Adv. Mater.* **2013**, *25*, 3526.

[10] K. J. Yu, D. Kuzum, S. W. Hwang, B. H. Kim, H. Juul, N. H. Kim, S. M. Won, K. Chiang, M. Trumpis, A. G. Richardson, H. Cheng, H. Fang, M. Thompson, H. Bink, D. Talos, K. J. Seo, H. N. Lee, S. K. Kang, J. H. Kim, J. Y. Lee, Y. Huang, F. E. Jensen, M. A. Dichter, T. H. Lucas, J. Viventi, B. Litt, J. A. Rogers, *Nat. Mater.* **2016**, *15*, 782.

[11] K. Jensen, M. Larsen, S. H. Nielsen, L. B. Larsen, K. S. Olsen, R. N. Jørgensen, *Robotics* **2014**, *3*, 207.

[12] T. Duckett, S. Pearson, S. Blackmore, B. Grieve, W.-H. Chen, G. Cielniak, J. Cleaversmith, J. Dai, S. Davis, C. Fox, P. From, I. Georgilas, R. Gill, I. Gould, M. Hanheide, A. Hunter, F. Iida, L. Mihalyova, S. Nefti-Meziani, G. Neumann, P. Paoletti, T. Pridmore, D. Ross, M. Smith, M. Stoelen, M. Swainson, S. Wane, P. Wilson, I. Wright, G.-Z. Yang, *arXiv* **2018**, 1806.06762.

[13] R. R. Shamshiri, C. Weltzien, I. A. Hameed, I. J. Yule, T. E. Grift, S. K. Balasundram, L. Pitonakova, D. Ahmad, G. Chowdhary, *Int. J. Agric. Biol. Eng.* **2018**, *11*, 1.

[14] L. Švorc, M. Rievaj, D. Bustin, *Sensors Actuators, B Chem* **2013**, *181*, 294.

[15] R. Akram, Natasha, S. F., M. Z. Hashmi, A. Wahid, M. Adnan, M. Mubeen, N. Khan, M. I. A. Rehmani, M. Awais, M. Abbas, K. Shahzad, S. Ahmad, H. M. Hammad, W. Nasim, *Environ. Sci. Pollut. Res.* **2019**, *26*, 16923.

[16] D. E. Meyer, J. P. Katz, *J. Clean. Prod.* **2016**, *112*, 369.

[17] J. Zhou, Y. Li, L. Xie, R. Xu, R. Zhang, M. Gao, W. Tian, *Mater. Today Energy* **2021**, *21*, 100712.

[18] R. Zhang, Y. Li, L. Qiao, D. Li, J. Deng, J. Zhou, L. Xie, Y. Hou, T. Wang, W. Tian, J. Cao, F. Cheng, B. Yang, K. Liang, P. Chen, B. Kong, *Energy Storage Mater.* **2021**, *37*, 123.

[19] W. Tian, Y. Li, J. Zhou, T. Wang, R. Zhang, J. Cao, M. Luo, N. Li, N. Zhang, H. Gong, J. Zhang, L. Xie, B. Kong, *ACS Appl. Mater. Interfaces* **2021**, *13*, 8285.

[20] R. Dubey, V. Guruviah, *Ionics (Kiel)* **2019**, *3*,18.

[21] P. L. Huang, X. F. Luo, Y. Y. Peng, N. W. Pu, M. Der Ger, C. H. Yang, T. Y. Wu, J. K. Chang, *Electrochim. Acta* **2015**, *161*, 371.

[22] E. Kovalska, C. Kocabas, *Mater. Today Commun.* **2016**, *7*, 155.

[23] Z. S. Iro, C. Subramani, S. S. Dash, *Int. J. Electrochem. Sci.* **2016**, *11*, 10628.

[24] R. Wang, Q. R. Wang, M. J. Yao, K. N. Chen, X. Y. Wang, L. L. Liu, Z. Q. Niu, J. Chen, *Rare Met.* **2018**, *37*, 536.

[25] Z. Niu, L. Zhang, L. Liu, B. Zhu, H. Dong, X. Chen, *Adv. Mater.* **2013**, *25*, 4035.

[26] X. Pu, M. Liu, L. Li, S. Han, X. Li, C. Jiang, C. Du, J. Luo, W. Hu, Z. L. Wang, *Adv. Energy Mater.* **2016**, *6*, 1601254.

[27] G. Wu, P. Tan, D. Wang, Z. Li, L. Peng, Y. Hu, C. Wang, W. Zhu, S. Chen, W. Chen, *Sci. Rep.* **2017**, *7*, 1.

[28] S. Huang, X. Zhu, S. Sarkar, Y. Zhao, *APL Mater.* **2019**, *7*, 100901.

[29] H. Li, D. Yuan, C. Tang, S. Wang, J. Sun, Z. Li, T. Tang, F. Wang, H. Gong, C. He, *Carbon N. Y.* **2016**, *100*, 151.

[30] C. Chen, Y. Zhang, Y. Li, J. Dai, J. Song, Y. Yao, Y. Gong, I. Kierzewski, J. Xie, L. Hu, *Energy Environ. Sci.* **2017**, *10*, 538.

[31] Q. Niu, Y. Guo, K. Gao, Z. Shao, *RSC Adv.* **2016**, *6*, 109143.

[32] R. Mantravadi, P. R. Chinnam, D. A. Dikin, S. L. Wunder, *ACS Appl. Mater. Interfaces* **2016**, *8*, 13426.

[33] W. G. Moon, G. P. Kim, M. Lee, H. D. Song, J. Yi, *ACS Appl. Mater. Interfaces* **2015**, *7*, 3503.

[34] R. Oraon, A. De Adhikari, S. K. Tiwari, G. C. Nayak, *ACS Sustainable Chem. Eng.* **2016**, *4*, 1392.

[35] K. Aschberger, H. J. Johnston, V. Stone, R. J. Aitken, S. M. Hankin, S. A. K. Peters, C. L. Tran, F. M. Christensen, *Crit. Rev. Toxicol.* **2010**, *40*, 759.

[36] F. Poli, D. Momodu, G. E. Spina, A. Terella, B. K. Mutuma, M. L. Focarete, N. Manyala, F. Soavi, *Electrochim. Acta* **2020**, *338*, 135872.

[37] M. Salanne, *Top. Curr. Chem.* **2017**, *375*, 63.

[38] S. Zhang, N. Sun, X. He, X. Lu, X. Zhang, *J. Phys. Chem. Ref. Data* **2006**, *35*, 1475.

[39] P. L. Huang, X. F. Luo, Y. Y. Peng, N. W. Pu, M. Der Ger, C. H. Yang, T. Y. Wu, J. K. Chang, *Electrochim. Acta* **2015**, *161*, 371.

[40] D. J. Couling, R. J. Bernot, K. M. Docherty, J. N. K. Dixon, E. J. Maginn, *Green Chem.* **2006**, *8*, 82.

[41] S. Studzińska, B. Buszewski, *Anal. Bioanal. Chem.* **2009**, *393*, 983.

[42] A. Latała, P. Stepnowski, M. Nędzi, W. Mrozik, *Aquat. Toxicol.* **2005**, *73*, 91.

[43] I. F. Mena, E. Diaz, J. Palomar, J. J. Rodriguez, A. F. Mohedano, *Chemosphere* **2020**, *240*, 124947.

[44] D. Zhao, C. Chen, Q. Zhang, W. Chen, S. Liu, Q. Wang, Y. Liu, J. Li, H. Yu, *Adv. Energy Mater.* **2017**, *7*, 1700739.

[45] G. Lee, S. K. Kang, S. M. Won, P. Gutruf, Y. R. Jeong, J. Koo, S. S. Lee, J. A. Rogers, J. S. Ha, *Adv. Energy Mater.* **2017**, *7*, 1700157.

[46] M. Hu, J. Wang, J. Liu, P. Wang, Y. Feng, H. Wang, N. Nie, Y. Wang, Y. Huang, *Energy Storage Mater.* **2019**, *21*, 174.

[47] H. Lee, G. Lee, J. Yun, K. Keum, S. Y. Hong, C. Song, J. W. Kim, J. H. Lee, S. Y. Oh, D. S. Kim, M. S. Kim, J. S. Ha, *Chem. Eng. J.* **2019**, *366*, 62.

[48] R. K. Pal, S. C. Kundu, V. K. Yadavalli, *ACS Appl. Mater. Interfaces* **2018**, *10*, 9620.

[49] Q. Yang, Z. Huang, X. Li, Z. Liu, H. Li, G. Liang, D. Wang, Q. Huang, S. Zhang, S. Chen, C. Zhi, *ACS Nano* **2019**, *13*, 8275.

[50] C. Boehler, Z. Aqrawe, M. Asplund, *Bioelectron. Med.* **2019**, *2*, 89.

[51] Y. Han, L. Dai, *Macromol. Chem. Phys.* **2019**, *220*, 1800355.

[52] G. A. Snook, P. Kao, A. S. Best, *J. Power Sources* **2011**, *196*, 1.

[53] M. Yassine, D. Fabris, *Energies* **2017**, *10*, 1340.

[54] D. Li, W. Y. Lai, Y. Z. Zhang, W. Huang, *Adv. Mater.* **2018**, *30*, 1704738.

[55] T. Cheng, Y. W. Wu, Y. L. Chen, Y. Z. Zhang, W. Y. Lai, W. Huang, *Small* **2019**, *15*, e1901830.

[56] A. D. Valentine, T. A. Busbee, J. W. Boley, J. R. Raney, A. Chortos, A. Kotikian, J. D. Berrigan, M. F. Durstock, J. A. Lewis, *Adv. Mater.* **2017**, *29*, 1703817.

[57] D. Li, X. Liu, X. Chen, W. Y. Lai, W. Huang, *Adv. Mater. Technol.* **2019**, *4*, 1900196.

[58] L. Nayak, S. Mohanty, S. K. Nayak, A. Ramadoss, *J. Mater. Chem. C* **2019**, *7*, 8771.

[59] K. Wegner, P. Piseri, H. V. Tafreshi, P. Milani, *J. Phys. D.: Appl. Phys.* **2006**, *39*, R439.

[60] C. Ghisleri, F. Borghi, L. Ravagnan, A. Podestà, C. Melis, L. Colombo, P. Milani, *J. Phys. D.: Appl. Phys.* **2014**, *47*, 015301.

[61] V. N. Popok, O. Kylián, *Appl. Nano* **2020**, *1*, 25.

[62] F. Borghi, M. Milani, L. G. Bettini, A. Podestà, P. Milani, *Appl. Surf. Sci.* **2019**, *479*, 395.

[63] A. Podestà, G. Bongiorno, P. E. Scopelliti, S. Bovio, P. Milani, C. Semprebon, G. Mistura, *J. Phys. Chem. C* **2009**, *113*, 18264.

[64] G. Corbelli, C. Ghisleri, M. Marelli, P. Milani, L. Ravagnan, *Adv. Mater.* **2011**, *23*, 4504.

[65] T. Dotan, Y. Berg, L. Migliorini, S. M. Villa, T. Santaniello, P. Milani, Y. Shacham-Diamand, *Microelectron. Eng.* **2021**, *237*, 111478.

[66] L. G. Bettini, A. Bellacicca, P. Piseri, P. Milani, *Flex. Print. Electron.* **2017**, *2*, 025002.

[67] L. G. Bettini, P. Piseri, F. De Giorgio, C. Arbizzani, P. Milani, F. Soavi, *Electrochim. Acta* **2015**, *170*, 57.

[68] T. Santaniello, L. Migliorini, Y. Yan, C. Lenardi, P. Milani, *J. Nanoparticle Res.* **2018**, *20*, 250.

[69] T. Santaniello, L. Migliorini, F. Borghi, Y. Yan, S. Rondinini, C. Lenardi, P. Milani, *Smart Mater. Struct.* **2018**, *27*, 065004.

[70] L. Migliorini, T. Santaniello, S. Rondinini, P. Saettone, M. Comes Franchini, C. Lenardi, P. Milani, *Sensors Actuators, B Chem* **2019**, *286*, 230.

[71] S. M. Villa, V. M. Mazzola, T. Santaniello, E. Locatelli, M. Maturi, L. Migliorini, I. Monaco, C. Lenardi, M. Comes Franchini, P. Milani, *ACS Macro Lett.* **2019**, *8*, 414.

[72] Y. Yan, T. Santaniello, L. G. Bettini, C. Minnai, A. Bellacicca, R. Porotti, I. Denti, G. Faraone, M. Merlini, C. Lenardi, P. Milani, *Adv. Mater.* **2017**, *29*, 1606109.

[73] A. Jordan, N. Gathergood, *Chem. Soc. Rev.* **2015**, *44*, 8200.

[74] Y. Z. Zhang, Y. Wang, T. Cheng, L. Q. Yao, X. Li, W. Y. Lai, W. Huang, *Chem. Soc. Rev.* **2019**, *48*, 3229.

[75] M. J. Bleda-Martínez, J. A. Maciá-Agulló, D. Lozano-Castelló, E. Morallón, D. Cazorla-Amorós, A. Linares-Solano, *Carbon N. Y.* **2005**, *43*, 2677.

[76] N. C. Osti, B. Dyatkin, M. W. Thompson, F. Tiet, P. Zhang, S. Dai, M. Tyagi, P. T. Cummings, Y. Gogotsi, D. J. Wesolowski, E. Mamontov, *Phys. Rev. Mater.* **2017**, *1*, 035402.

[77] N. Muhammad, M. I. Hossain, Z. Man, M. El-Harbawi, M. A. Bustam, Y. A. Noaman, N. B. Mohamed Alitheen, M. K. Ng, G. Hefter, C. Y. Yin, *J. Chem. Eng. Data* **2012**, *57*, 2191.

[78] P. Piseri, H. V. Tafreshi, P. Milani, *Curr. Opin. Solid State Mater. Sci.* **2004**, *8*, 195.

[79] E. Barborini, S. Vinati, M. Leccardi, P. Repetto, G. Bertolini, O. Rorato, L. Lorenzelli, M. Decarli, V. Guarnieri, C. Ducati, P. Milani, *J. Micromechanics Microengineering* **2008**, *18*, 055015.

[80] E. Barborini, P. Piseri, A. Podesta', P. Milani, *Appl. Phys. Lett.* **2000**, *77*, 1059.

[81] F. Caruso, A. Bellacicca, P. Milani, *Appl. Phys. Lett.* **2016**, *108*, 163501.

[82] L. G. Bettini, G. Bardizza, A. Podestà, P. Milani, P. Piseri, *J. Nanoparticle Res.* **2013**, *15*, 1429.

[83] L. G. Bettini, G. Divitini, C. Ducati, P. Milani, P. Piseri, *Nanotechnology* **2014**, *25*, 435401.

[84] Z. Yi, L. G. Bettini, G. Tomasello, P. Kumar, P. Piseri, I. Valitova, P. Milani, F. Soavi, F. Cicoira, *J. Polym. Sci. Part B Polym. Phys.* **2017**, *55*, 96.

[85] C. Piazzoni, P. Milani, in *Spark Ablation: Building Blocks for Nanotechnology*, (Eds: A. Schmidt-Ott), CRC Press, Boca Raton, FL **2019**, Ch. 8.